

## Aboveground forest biomass derived using multiple dates of WorldView-2 stereo-imagery: quantifying the improvement in estimation accuracy

Mikko Vastaranta, Xiaowei Yu, Ville Luoma, Mika Karjalainen, Ninni Saarinen, Michael A. Wulder, Joanne C. White, Henrik J. Persson, Markus Hollaus, Tuomas Yrttimaa, Markus Holopainen & Juha Hyyppä

To cite this article: Mikko Vastaranta, Xiaowei Yu, Ville Luoma, Mika Karjalainen, Ninni Saarinen, Michael A. Wulder, Joanne C. White, Henrik J. Persson, Markus Hollaus, Tuomas Yrttimaa, Markus Holopainen & Juha Hyyppä (2018): Aboveground forest biomass derived using multiple dates of WorldView-2 stereo-imagery: quantifying the improvement in estimation accuracy, International Journal of Remote Sensing, DOI: [10.1080/01431161.2018.1492176](https://doi.org/10.1080/01431161.2018.1492176)

To link to this article: <https://doi.org/10.1080/01431161.2018.1492176>



© 2018 Informa UK Limited, trading as Taylor & Francis Group



Published online: 11 Jul 2018.



Submit your article to this journal [↗](#)





Article views: 291



View Crossmark data [↗](#)

## Aboveground forest biomass derived using multiple dates of WorldView-2 stereo-imagery: quantifying the improvement in estimation accuracy

Mikko Vastaranta <sup>a,b,c</sup>, Xiaowei Yu<sup>b,d</sup>, Ville Luoma<sup>a,b</sup>, Mika Karjalainen<sup>d</sup>, Ninni Saarinen <sup>a,b,c</sup>, Michael A. Wulder <sup>e</sup>, Joanne C. White <sup>e</sup>, Henrik J. Persson <sup>f</sup>, Markus Hollaus<sup>g</sup>, Tuomas Yrttimaa<sup>a,b</sup>, Markus Holopainen<sup>a,b</sup> and Juha Hyypä<sup>b,d</sup>

<sup>a</sup>Department of Forest Sciences, University of Helsinki, Helsinki, Finland; <sup>b</sup>Centre of Excellence in Laser Scanning Research, Finnish Geospatial Research Institute, Masala, Finland; <sup>c</sup>School of Forest Sciences, University of Eastern Finland, Joensuu, Finland; <sup>d</sup>Department of Remote Sensing and Photogrammetry, Finnish Geospatial Research Institute, Masala, Finland; <sup>e</sup>Canadian Forest Service (Pacific Forestry Centre), Natural Resources Canada, Victoria, BC, Canada; <sup>f</sup>Department of Forest Resource Management, Swedish University of Agricultural Sciences, Umeå, Sweden; <sup>g</sup>Department of Geodesy and Geoinformation, Vienna University of Technology, Vienna, Austria

### ABSTRACT

The aim of this study was to investigate the capabilities of two date satellite-derived image-based point clouds (IPCs) to estimate forest aboveground biomass (AGB). The data sets used include panchromatic WorldView-2 stereo-imagery with 0.46 m spatial resolution representing 2014 and 2016 and a detailed digital elevation model derived from airborne laser scanning data. Altogether, 332 field sample plots with an area of 256 m<sup>2</sup> were used for model development and validation. Predictors describing forest height, density, and variation in height were extracted from the IPC 2014 and 2016 and used in *k*-nearest neighbour imputation models developed with sample plot data for predicting AGB. AGB predictions for 2014 (AGB<sub>2014</sub>) were projected to 2016 using growth models (AGB<sub>Projected\_2016</sub>) and combined with the AGB estimates derived from the 2016 data (AGB<sub>2016</sub>). AGB prediction model developed with 2014 data was also applied to 2016 data (AGB<sub>2016\_pred2014</sub>). Based on our results, the change in the 90<sup>th</sup> percentile of height derived from the WorldView-2 IPC was able to characterize forest height growth between 2014 and 2016 with an average growth of 0.9 m. Features describing canopy cover and variation in height derived from the IPC were not as consistent. The AGB<sub>2016</sub> had a bias of -7.5% (-10.6 Mg ha<sup>-1</sup>) and root mean square error (RMSE) of 26.0% (36.7 Mg ha<sup>-1</sup>) as the respective values for AGB<sub>Projected\_2016</sub> were 7.0% (9.9 Mg ha<sup>-1</sup>) and 21.5% (30.8 Mg ha<sup>-1</sup>). AGB<sub>2016\_pred2014</sub> had a bias of -19.6% (-27.7 Mg ha<sup>-1</sup>) and RMSE of 33.2% (46.9 Mg ha<sup>-1</sup>). By combining predictions of AGB<sub>2016</sub> and AGB<sub>Projected\_2016</sub> at sample plot level as a weighted average, we were able to decrease the bias notably compared to estimates made on any single date. The lowest bias of -0.25% (-0.4 Mg ha<sup>-1</sup>) was obtained when equal weights of 0.5 were given to the AGB<sub>Projected\_2016</sub> and AGB<sub>2016</sub> estimates. Respectively, RMSE of 20.9% (29.5 Mg ha<sup>-1</sup>) was obtained using

### ARTICLE HISTORY

Received 2 June 2017  
Accepted 13 June 2018

**CONTACT** Mikko Vastaranta  mikko.vastaranta@uef.fi  Department of Forest Sciences, University of Helsinki, 00014 Helsinki, Finland

© 2018 Informa UK Limited, trading as Taylor & Francis Group

This is an Open Access article distributed under the terms of the Creative Commons Attribution-NonCommercial-NoDerivatives License (<http://creativecommons.org/licenses/by-nc-nd/4.0/>), which permits non-commercial re-use, distribution, and reproduction in any medium, provided the original work is properly cited, and is not altered, transformed, or built upon in any way.

equal weights. Thus, we conclude that combination of two date WorldView-2 stereo-imagery improved the reliability of AGB estimates on sample plots where forest growth was the only change between the two dates.

## 1. Introduction

Sustainable forest management practices and studies of forest function require up-to-date estimates of biomass. Further, forest biomass estimates can be required outside of the typically inventoried land-base (i.e. non-merchantable or remote locations) or out of sync with inventory cycles. As such, additional remote-sensing-based opportunities to capture biomass are required. Forest aboveground biomass (AGB) is often mapped using medium-resolution satellite imagery (Song 2013), such as Landsat and Sentinel-2, which provide open-access optical data with many acquisition opportunities per year (Drusch et al. 2012; Wulder et al. 2012a). Issues and options for using higher spatial resolution imagery to provide more detailed information on forest ecosystems (Wulder et al. 2004) and more specifically on forest inventory parameters have also been explored (as reviewed in Falkowski et al. 2009). AGB is among the forest inventory attributes that is highly correlated with vegetation height and density (Koch 2010; Zolkos, Goetz, and Dubayah 2013); as a result, single date three-dimensional (3D) remote-sensing techniques from air- and spaceborne platforms have proven to outperform optical techniques for measuring or predicting this forest structural characteristic (Hyypä et al. 2008; Koch 2010; Kaasalainen et al. 2015; Wulder et al. 2012b; Yu et al. 2015). However, forest AGB is a dynamic attribute that changes over time due to natural forest dynamics associated with growth and disturbances, or due to human activities such as harvesting or land-use change. Therefore, mapping and monitoring of forest AGB over time is dependent on both spatial and temporal resolutions of the sensor under consideration (Goetz et al. 2009). In addition to data availability and consistency requirements, data analysis methods capable of taking advantage of multi-temporal data are essential for forest AGB monitoring.

Currently, most of the 3D data used for detailed mapping of forest inventory attributes (including AGB) are collected using airborne laser scanning (ALS, e.g. Yu et al. 2015) although more and more alternative options are emerging (e.g. White et al. 2013; Yu et al. 2015). One of these alternatives for providing structural 3D information from forests is an automated stereogrammetric processing of very high spatial resolution (VHSR; i.e. <1 m) satellite imagery. VHSR satellite imagery have been available commercially for over a decade (Falkowski et al. 2009) and have been used for deriving forest AGB via analyses of shadow fraction (Leboeuf et al. 2007), spectral information (Hyde et al. 2006), image texture (Proisy, Coutron, and Fromard 2007), and individual tree crown segmentation (Greenberg, Dobrowski, and Ustin 2005). However, due to the lack of a third dimension, the AGB maps obtained using VHSR satellite imagery have not been sufficiently accurate to support forest management (Holopainen, Vastaranta, and Hyypä 2014). Moreover, compared to medium-resolution satellite imagery, the higher cost and greater processing overhead associated with the use of VHSR satellite imagery

has limited its application to a sample basis for large-area forest characterization (i.e. to support sample-based national forest inventories; Falkowski et al. 2009). In addition, until recent improvements in automatic image matching methods (e.g. White et al. 2013) and the growing availability of the detailed ALS-derived digital terrain models (DTMs,) it has not been possible to obtain features describing canopy height automatically from VHSR satellite imagery.

Detailed mapping information is often used for planning of forest management as well as for planning of forest operations (Holopainen, Vastaranta, and Hyyppä 2014). Compared to ALS, VHSR satellite imagery-derived 3D information can provide improved temporal resolution with only slightly lower prediction accuracies for forest inventory attributes (Yu et al. 2015). It has been assumed that in countries applying intensive forestry, there will be a frequent flow of optical data, coupled with data from 3D sensors to support AGB mapping and monitoring. Examples of this type of data flow are presented in Holopainen, Vastaranta, and Hyyppä (2014) and Nyström et al. (2015) and they include the potential availability of several optical and radar satellite images per year, point clouds from digital photogrammetry acquired every few years, and ALS data acquired at time interval from 5 to 10 years. Thus, in addition to improvements in spatial resolution (i.e. ground sampling distances (GSDs) of digital photogrammetry, point density of ALS data, and resolution of the digital surface model), the temporal density will be enhanced as well. It should be pointed out that with most of the 3D remote-sensing methods, it is a crucial prerequisite to have a detailed DTM available, which usually requires an ALS data acquisition at least once. WorldView-2 is one optical satellite sensor that has shown great potential providing data suitable to generate stereo-matched 3D heights that are relevant for forest applications (Immitzer et al. 2016; Persson and Perko 2016; Straub et al. 2013; Yu et al. 2015). WorldView-2 acquires panchromatic images with 0.46 m GSD at nadir and eight multispectral bands at a reduced resolution (1.84 m GSD at nadir). Directable sensor head also supports collection of in-track stereo-imagery.

Even though multi-temporal data are becoming a viable source for obtaining forest resource information, the use of multi-temporal 3D data sets for forest mapping remains largely unexplored (e.g. Eitel et al. 2016; Holopainen, Vastaranta, and Hyyppä 2014; Nyström et al. 2015). For forest monitoring, data from two time-points have been used to detect changes in forest canopy structure (e.g. Honkavaara, Litkey, and Nurminen 2013; Vastaranta et al. 2012; Yu et al. 2004) and to estimate forest stand age (Vastaranta et al. 2016). In data fusion applications (e.g. forest mapping), data from two sensors can be used to calculate additional metrics to be further used in building predictive models for forest attributes (Kaasalainen et al. 2015).

The main aim of this study is to quantify the potential improvements in AGB estimation that may be realized through the combination of two independent estimates of AGB, derived at two different points in time. We focused our analyses on forest AGB because sustainable forest management practices, carbon assessments, and studies of forest functions require up-to-date estimates of biomass. In our study, we first predicted plot-level estimates of AGB for 2014 ( $AGB_{2014}$ ) and 2016 ( $AGB_{2016}$ ) using an AGB measurements from sample plots and information on vertical forest structure. Information on forest vertical structure was derived from point clouds generated from WorldView-2 stereo-imagery. We then explored how the prediction accuracy for AGB in

2016 could be improved by incorporating the 2014 AGB estimates. One of our objectives was, therefore, to evaluate the degree of correlation between the AGB prediction errors for both inventory years. In addition, we applied the prediction model developed with the 2014 data to the data collected in 2016 to test the transferability of the prediction model between two data acquisitions. We concentrated our analyses on sample plots where forest growth was the only change between the two dates.

## 2. Materials and methods

### 2.1. Study area

The study area is in Evo, Finland (61.19° N, 25.11° E), approximately 145 km from Helsinki (Figure 1). The area belongs to the southern boreal forest zone and comprises approximately 2000 ha of mostly managed forest. However, Evo is also a national hiking area, and thus represents a range of stand conditions from close to natural state forests to managed forests. Stands are mainly even aged and single layer, with an average size of slightly less than 1 ha. The elevation of the area varies from 125 m to 185 m above sea level. Scots pine (*Pinus sylvestris* L.) and Norway spruce (*Picea abies* (L.) H. Karst.) are the dominant tree species in the study area.

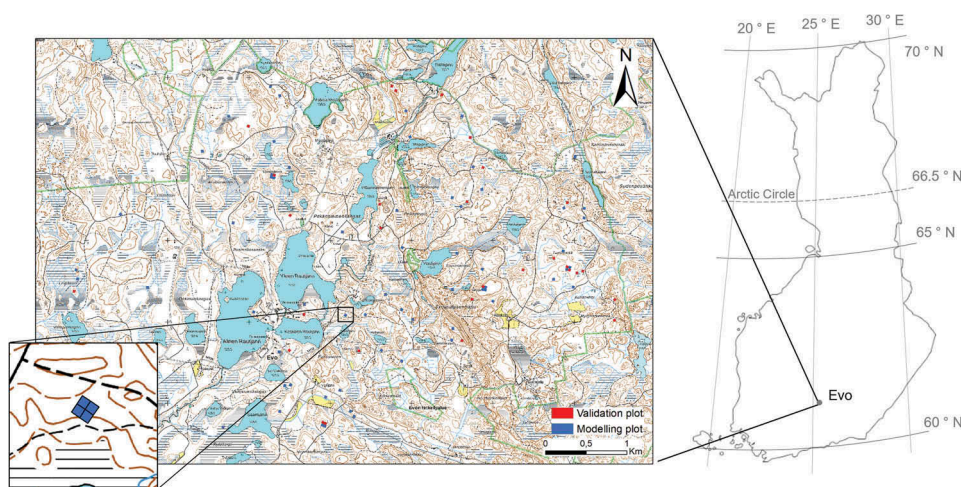


**Figure 1.** Location of the study area and sample plots in southern Finland. The total number of sample plots ( $n = 364$ ) is comprised of 91 sample plot clusters.

### 2.2. Approach

In our study design, we produced four different AGB estimates for the year 2016 (Figure 2). First, we produced separate plot-level estimates of AGB for 2014 ( $AGB_{2014}$ ) and 2016 ( $AGB_{2016}$ ) using WorldView-2 satellite imagery in an area-based approach (ABA). The ABA prediction of AGB is based on a statistical dependency between predictor variables derived from WorldView-2 imagery and AGB measured from sample plots. After generating our two separate estimates of AGB ( $AGB_{2014}$  and  $AGB_{2016}$ ), we

projected the growth from  $AGB_{2014}$  over two years to 2016 ( $AGB_{Projected\_2016}$ ). To explore how the prediction accuracy for AGB in 2016 could be improved by incorporating the 2014 AGB estimates, we calculated a combined estimate for 2016 ( $AGB_{Combined\_2016}$ ) as a weighted average. Then, we also applied the prediction model developed with the 2014 data to the data collected in 2016 ( $AGB_{2016\_pred2014}$ ) to test the transferability of the prediction model between two data acquisitions. Finally, our four estimates of AGB for 2016 were compared to the sample plot estimates that were used as reference.

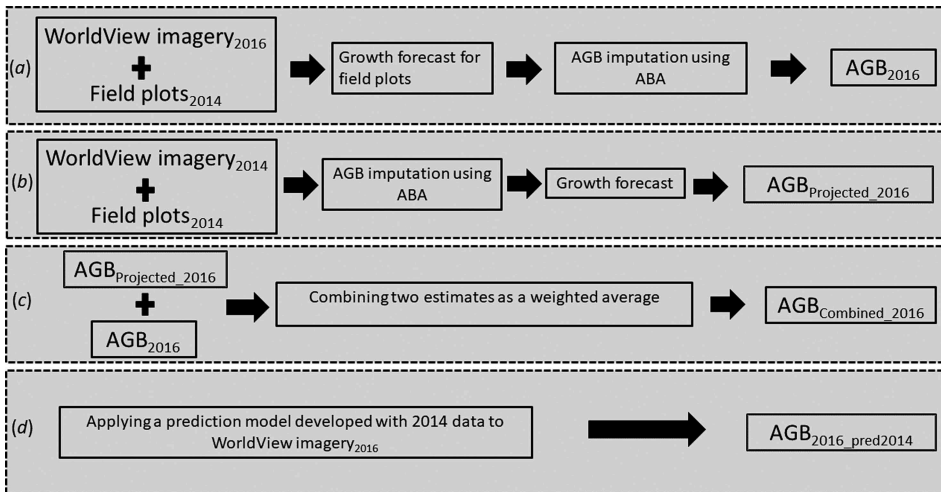


**Figure 2.** Workflow for obtaining four different aboveground biomass (AGB) estimates for year 2016. Area-based approach (ABA) was used to predict AGB for each plot in 2014 ( $AGB_{2014}$ ) and (a) 2016 ( $AGB_{2016}$ ). Then (b)  $AGB_{2014}$  estimates were growth projected to 2016 ( $AGB_{Projected\_2016}$ ) and (c) combined with  $AGB_{2016}$  ( $AGB_{Combined\_2016}$ ). (d) AGB prediction model developed with 2014 data was also applied to 2016 data ( $AGB_{2016\_pred2014}$ ). Accuracies of  $AGB_{2016}$ ,  $AGB_{Projected\_2016}$ ,  $AGB_{Combined\_2016}$ , and  $AGB_{2016\_pred2014}$  were validated at sample plot level.

### 2.3. Sample plots used for model development and validation

In total, 364 rectangular sample plots with 256 m<sup>2</sup> area were mapped and measured in the field during summer of 2014. Respective sample plot size is used in ALS-based forest-mapping inventories in Finland. The sample plot locations were selected based on the existing ALS data collected by National Land Survey of Finland in 2012 to represent the variation in canopy heights and densities in the study area. For improving efficiency of the field measurements, sample plots were clustered. The total sample plot number of 364 is therefore comprised of 91 sample plot clusters, with four sample plots per cluster. Accurate sample plot locations were measured using a Trimble total station (5602S DR200+, Trimble, Inc., Sunnyvale, CA, USA), which was oriented to ETRS-TM35FIN coordinate system using ground control points (GCPs) measured with VRS-GNSS (R8, Trimble, USA) on open areas close to each plot. From the sample plots, all trees having a diameter-at-breast height (DBH) larger than 5 cm were identified for species and measured with steel calipers from two

directions perpendicular to each other and the DBH was calculated as the mean of the two. Tree height was measured using an electronic hypsometer (Vertex IV, Haglöf, Sweden) from all the trees as well. Precision of DBH and height measurements are expected to be approximately 0.3 cm and 0.5 m, respectively, based on our evaluations (Luoma et al. 2017). The AGB for each tree was calculated using the allometric equations with tree species, DBH, and height as inputs (Repola 2008, 2009). In our study area, root mean square error (RMSE) of these equations has varied from 18% to 29% at tree level (Kankare et al. 2013; Yu et al. 2013). The AGB for a sample plot was obtained by summing the tree level AGBs. Subsequently, the sample plots were divided into two sets: one to be used in model development for ABA and the other to be used for validation of the derived models. The plot selection was conducted by considering the variation of basal area weighted mean height ( $H_g$ ) and basal area ( $G$ ) among the sample plots.  $H_g$  and  $G$  were derived for each sample plot based on field-measured DBHs and heights;  $H_g$  ranged from 7.9 m to 31.5 m and  $G$  from 3.7 m<sup>2</sup> ha<sup>-1</sup> to 55 m<sup>2</sup> ha<sup>-1</sup>. Sample plots of the same sample plot cluster were all used either for modelling or validation. We visited each sample plot in the field in 2016 and detected forest operations and disturbances that had taken place between 2014 and 2016. The majority of these detected changes were thinnings (84%). Due to the detected changes, our final sample plot data sets included 84 validation plots and consequently, 248 and 204 sample plots to be used in the modelling with 2014 and 2016 WorldView-2 imagery, respectively (Table 1). The AGB derived from the sample plot data was updated from 2014 to the year 2016 by using the SIMO (Simulation and Optimization) forest growth simulator (Rasinmäki, Mäkinen, and Kalliovirta 2009) applying the existing growth models for Finnish forests (Hynynen et al. 2002). Thus, it should be noted that the AGB reference values used in 2016 included growth-projection error.

#### 2.4. Digital terrain model from airborne laser scanning

ALS data used for DTM generation were acquired on 5 September 2014, using a Leica ALS70-HA SN7202 system (Leica Geosystems AG, Heerbrugg, Switzerland). The data were collected from an altitude of 900 m, resulting in an average pulse density of approximately 6 pulses per m<sup>2</sup>. ALS data were geo-referenced in the ETRS-TM35FIN coordinate system and calibrated for heading, pitch, and roll by the data provider. Afterwards, the ALS data were first classified into ground or non-ground points using the standard approach of the TerraScan based on a triangulated irregular network (Axelsson 2000). A DTM with a resolution of 1 m was then generated using the classified ground points.

**Table 1.** The descriptive statistics of the aboveground biomass (AGB, Mg ha<sup>-1</sup>) variation within the modelling and validation sample plots in 2014 and 2016.

Sample plot set	Year	<i>n</i>	Minimum	Mean	Maximum	Standard deviation
Modelling	2014	248	11.6	132.5	312.1	54.5
Validation	2014	84	39.2	137.0	238.5	50.6
Modelling	2016	204	12.7	138.4	311.5	54.3
Validation	2016	84	42.3	141.3	242.2	53.3

## 2.5. Worldview-2 stereo-imagery and point cloud processing for 2014 and 2016

The optical satellite images used here were acquired from the WorldView-2 satellite because of its possibility to obtain in-track stereo pairs with a VHSR (i.e. <1 m). WorldView-2 is a commercial optical satellite owned and operated by Digital Globe and it was launched in October 2009 providing panchromatic images with the GSD of 0.46 m at nadir. While not used in this study, WorldView-2 also provides multispectral images at a GSD of 1.84 m. Cloud-free image pairs were acquired on 11 July 2014 and 13 September 2016, covering the entire study area. The goal was to have the stereo-image pair for 2016 as close the acquisition date of 2014 (i.e. in July) as possible; however, because of cloudiness in 2016 this turned out to be impossible. The basic information of the WorldView-2 image pairs is presented in Table 2. The geo-positioning accuracy of WorldView-2 image pair was good; however, there was a clear need to refine geo-positioning using GCPs. The Socet Set software was used and 10 well-identifiable GCPs were digitized from the images. Then, the DTM from ALS was used to extract 3D ground coordinates for the GCPs. The resulting RMSE of the triangulation solution was 0.3 m, which is below the pixel size. The automatic matching of image pairs in the calculation of 3D surface points was carried out using the NGATE (next-generation automatic terrain extraction) module of the Socet Set workstation (DeVenecia, Walker, and Zhang 2007). Because the goal of the present study was not to develop new methods for image matching, and the WorldView-2 stereo-images were supported in the Socet Set software, we decided to use NGATE for extracting surface models. NGATE uses area-based cross-correlation approach in image matching similarity measurements, but also uses edge features in matching to eliminate possible elevation discontinuities, which exist mainly in build-up areas (Zhang et al. 2006). Basically, the NGATE process is fully automatic and the user can guide the process by changing a few parameters related to the matching algorithm. The main parameters are used to control the number and accuracy of the resulting 3D points (i.e. successfully matched points between images). In the matching of WorldView-2 stereo-images, one default strategy (i.e. the urban canyon) was used after visual comparison of a selection of default NGATE strategies. According to the NGATE user's manual, the urban canyon strategy allows steep elevation changes (e.g. urban canyons in built-up area), which also exist in borders of the forested areas. Based on our visual inspection, in this case, the urban canyon strategy appeared to perform the best among other strategies. However, the differences between the default matching strategies in general were very small.

**Table 2.** Parameters of the used WorldView-2 image pairs.

Image	11 July 2014 (1)	11 July 2014 (2)	13 September 2016 (1)	13 September 2016 (2)
Mean in-track angle (°)	0.5	-11.6	9.1	-8.8
Mean cross-track angle (°)	-6.8	-7.1	11.1	10.5
Mean off-nadir angle (°)	6.8	13.6	14.3	13.7

## 2.6. Data co-registration and feature extraction

Besides the geometric correction before 3D point production, image-based point clouds (IPCs) were also visually inspected with respect to ALS point cloud, for possible horizontal



and vertical displacements. If such displacement existed, the difference was measured and corrected accordingly. The IPCs were then normalized by removing the ground elevation from intersected height values to obtain the height above ground using the DTM created from the ALS data. From the normalized point cloud data, the various height distribution and density-related features were calculated from the points above the 2 m threshold for grid cells corresponding to the location and area of the sample plots. First, some descriptive statistics were computed from points. These included maximum height ( $H_{\max}$ ), mean height calculated as the arithmetic mean of heights ( $H_{\text{mean}}$ ), mode of heights ( $H_{\text{mode}}$ ), standard deviation of the heights ( $H_{\text{std}}$ ), coefficient of variation ( $H_{\text{cv}}$ ), and penetration percentage ( $P$ ) as a ratio of ground points (i.e. points below 2 m) to total number of points. Second, the various percentiles were calculated from 10% to 90% of canopy height distribution with a 10% increment ( $H_{10}$ – $H_{90}$ ). Finally, each point cloud was divided into 10 equal intervals of height, starting at the bottom of the canopy (i.e. at the height of 2 m) and ending at the top, and then density feature was computed as a proportion of points in each interval to the total number of points ( $C_1$ – $C_{10}$ ). Detailed definitions and calculations are given in Table 3.

## 2.7. Predicting forest aboveground biomass for 2014 and 2016

### 2.7.1. Area-based approach with imputation

The 3D features extracted from the WorldView-2 IPCs described tree height, canopy cover, and variation in tree height at a sample plot. All these features are correlated with forest AGB (e.g. Kaasalainen et al. 2015; Koch 2010). The selection of the features was based on simple correlation analysis with the field-measured forest structural attributes (2014) and WorldView-2 IPC-derived features (2014). First, the features were classified into three categories depicting tree height, canopy cover, and variation in tree height (Table 3). From the first category, the feature that had the highest Pearson correlation coefficient with the maximum tree height measured in the field was selected for the AGB imputation model. Then, from the second category, the feature that had the highest Pearson correlation coefficient with the field-measured basal area was selected. However, before selection, the correlation between the two features (i.e. characterizing tree height and canopy cover) was investigated and if it was above 0.6, the feature correlating with the basal area was replaced with the feature having the second highest correlation coefficient. Finally, from the third category, the feature with the highest correlation with the standard deviation of the field-measured tree heights was found and added to the model after evaluating the correlation with the other two predictors (i.e. correlation <0.6). The selected predictors were used in the AGB imputations for both years obtaining separate AGB estimates for 2014 and 2016 ( $\text{AGB}_{2014}$  and  $\text{AGB}_{2016}$ ). Non-parametric nearest neighbour estimation method was used for predicting AGB for the sample plots. The optimal number of neighbours, varying from 1 to 9 with a step size of 2, was tested for both years separately. In our method, nearness of the neighbours in the feature space (using the selected features) was defined as the probability of ending up in the same terminal node in a random forest classification (Breiman 2001, see Hudak et al. 2008). For predicting forest AGB for a sample plot, we imputed forest AGB as well as species-specific  $G$ ,  $H_g$ , basal area-weighted mean diameter, and stem number from plots that were similar in the sense of features describing tree height, canopy cover, and variation in tree height (i.e. the selected features from WorldView-2 IPCs). Species-specific inventory attributes were required for growth update.

AGB imputations for 2014 were updated to 2016 (i.e. projected AGB estimates,  $AGB_{Projected\_2016}$ ) using the SIMO forest growth simulator (Rasinmäki, Mäkinen, and Kalliovirta 2009) in a similar way to sample plot data growth update. The AGB prediction model for 2014 was also applied to WorldView-2 data acquired in 2016 ( $AGB_{2016\_pred2014}$ ).

**Table 3.** Features extracted from the normalized digital surface model derived from WorldView-2 image-based point clouds and feature definitions.

Feature category	Feature	Definition
Tree height	$H_{max}$	Maximum of the normalized heights of all points
	$H_{mean}$	Arithmetic mean of normalized heights of all points above 2 m height threshold
	$H_{mod}$	Mode of normalized heights of all points above 2 m height threshold
	$H_{10-90}$	10% to 90% percentiles of normalized heights of all points above 2 m height threshold with a 10% increment
Canopy cover	$P$	$N_{H \leq 2} / N_{total} \times 100$ , where $N_{total}$ is the number of all points and $N_{H \leq 2}$ the number of points below and equal to 2 m height threshold
	$C_1-C_{10}$	$C_i = N_i / N_{total}$ , where $i = 1$ to 10, $N_i$ is the number of points within $i$ th layer when tree height was divided into 10 intervals starting from 2 m height, $N_{total}$ is the number of all points
Variation in tree heights	$H_{std}$	Standard deviation of normalized heights of all points above 2 m threshold
	$H_{cv}$	Coefficient of variation calculated as $H_{std} / H_{mean}$

### 2.7.2. Combining projected AGB estimate with the most recent estimate

Combined AGB estimates for 2016 ( $AGB_{Combined\_2016}$ ) were obtained for each sample plot by calculating the weighted average of  $AGB_{Projected\_2016}$  and the most recent estimate ( $AGB_{2016}$ ). We used equal weights of 0.5 for  $AGB_{Projected\_2016}$  and  $AGB_{2016}$  as a default. However, after calculating the combined estimates, we investigated if our presumption of equal weights was valid and tested varying weights between 0 and 1 with an interval of 0.1. These sensitivity tests were carried out using 84 validation plots. The same weights were used for all the sample plots.

### 2.7.3. Comparison of the different forest AGB estimates for year 2016

Validation of the four methods ( $AGB_{2016}$ ,  $AGB_{Projected\_2016}$ ,  $AGB_{Combined\_2016}$ , and  $AGB_{2016\_pred2014}$ ) was made by calculating the bias and RMSE for the AGB estimates using the 84 validation sample plots. For each method, the bias was calculated by subtracting the predicted value from the reference value. It should be noted that reference value included a 2 year growth update. RMSE was calculated based on differences between reference and predicted values. Bias and RMSE values relative to the mean reference AGB value (i.e. relative bias and RMSE, %) in the validation data were calculated as well. In addition, the correlations between AGB estimates for 2014 and 2016 ( $AGB_{2014}$  and  $AGB_{2016}$ ), as well as the correlation between estimation errors, were computed using Pearson correlation coefficient.

## 3. Results

### 3.1. Predictor selection

The feature  $H_{90}$  had the highest correlation (0.94) with the field-measured maximum tree height in the modelling data from 2014 ( $n = 248$ ). Correspondingly,  $P$  had the best

correlation ( $-0.51$ ) with the field-measured  $G$ , and  $H_{std}$  had the highest correlation ( $0.26$ ) with the variation in field-measured tree heights. Correlations between  $H_{90}$ ,  $P$ , and  $H_{std}$  remained below  $0.5$ , and therefore these features were selected to be further used in the AGB imputations for years 2014 and 2016.

Changes due to forest growth in  $H_{90}$  were on average  $0.9$  m and ranged from  $-4.3$  m to  $5.4$  m in undisturbed sample plots ( $n = 288$ , [Figure 3](#)). The change in canopy cover was on average  $-3.8\%$ , indicating that fewer points were detected below the threshold height of  $2$  m in 2016 than 2014. However, the variation in canopy cover change varied from  $-79.7\%$  to  $17.3\%$ , which shows that WorldView-2-based measurements can be inconsistent or saturate already at low levels of  $G$ . The change in  $H_{std}$  was on average  $-0.85$  m varying from  $-5.3$  m to  $3.1$  m. Based on the simulated forest growth for sample plots, the expected AGB growth was on average  $2.1$  Mg ha $^{-1}$  year $^{-1}$ , and, therefore, changes detected by analysing the features correspond well with the expected growth.

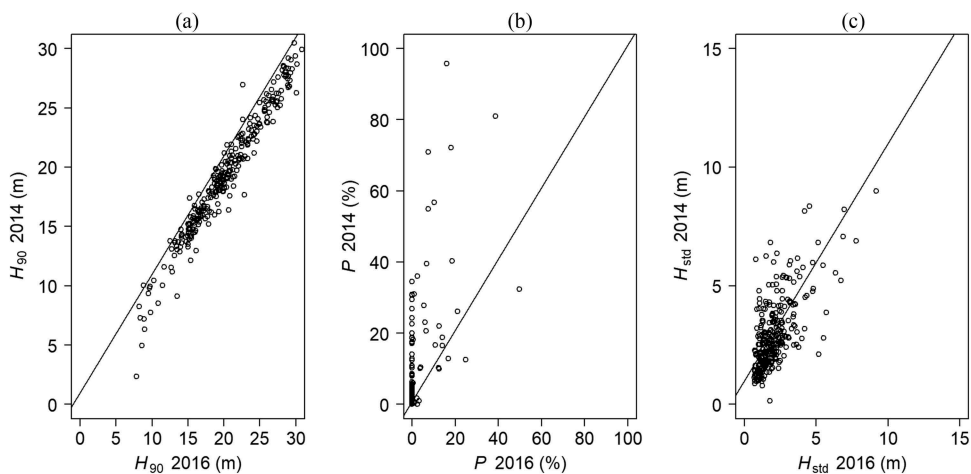


**Figure 3.** (a) 90th height percentile ( $H_{90}$ ), (b) penetration percentage ( $P$ ), and (c) standard deviation of height ( $H_{std}$ ) derived from WorldView-2 data for years 2014 and 2016.

### 3.2. Accuracy of the AGB estimates for 2014 and 2016

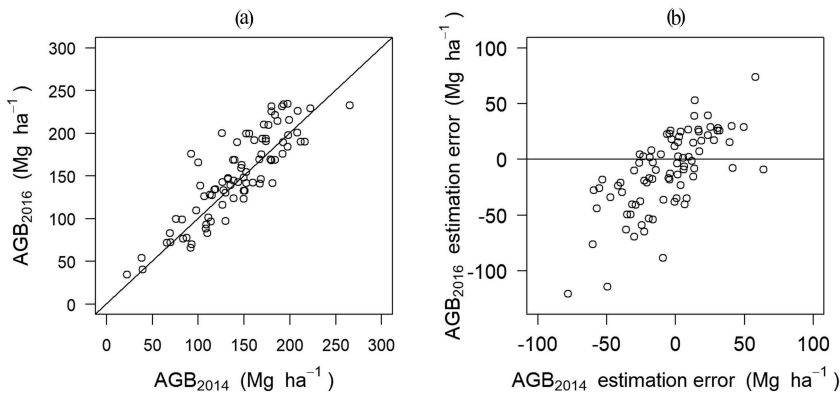
As shown in [Table 4](#), for 2014 the most accurate predictions for AGB were obtained by using seven nearest neighbours. In addition, use of seven neighbours provided comparable results achieved with other  $k$  values in terms of bias and standard deviation of the predicted values. Use of only the nearest neighbour ( $k = 1$ ) provided the lowest bias, and highest standard deviation in the predicted values, but most inaccurate estimates. Therefore, the use of seven nearest neighbours was selected from the inventory year 2014 for further analyses. In 2016, the most accurate predictions for AGB were obtained by using five nearest neighbours ([Table 5](#)). The lowest bias was also obtained with  $k = 5$ , and thus, the use of five nearest neighbours was selected for further analyses. The AGB predictions from both dates were

**Table 4.** Accuracy of the predicted aboveground biomass (AGB) estimates in validation sample plots ( $n = 84$ ) in 2014.

$k$	Bias ( $\text{mg ha}^{-1}$ )	Bias (%)	RMSE ( $\text{mg ha}^{-1}$ )	RMSE (%)	Standard deviation ( $\text{mg ha}^{-1}$ )
1	-3.7	-2.7	36.7	26.8	52.7
3	-7.0	-5.1	32.4	23.6	48.1
5	-6.7	-4.9	31.5	23.0	46.9
7	-6.1	-4.4	28.9	21.1	45.8
9	-7.7	-5.6	30.2	21.9	45.7

**Table 5.** Accuracy of the predicted aboveground biomass (AGB) estimates in validation sample plots ( $n = 84$ ) in 2016.

$k$	Bias ( $\text{mg ha}^{-1}$ )	Bias (%)	RMSE ( $\text{mg ha}^{-1}$ )	RMSE (%)	Standard deviation ( $\text{mg ha}^{-1}$ )
1	-14.2	-10.0	49.5	35.0	64.8
3	-12.9	-9.1	37.9	26.9	53.6
5	-10.6	-7.5	36.7	26.0	50.6
7	-11.6	-8.2	37.0	26.2	49.5
9	-12.3	-8.7	36.9	26.1	50.3

**Figure 4.** (a) Aboveground biomass prediction for 2014 ( $\text{AGB}_{2014}$ ) and 2016 ( $\text{AGB}_{2016}$ ) and (b) respective estimation errors at sample plot level.

highly correlated (Figures 4 and 5). The Pearson correlation coefficient calculated from the predictions was 0.86. Consequently, the errors between the two predictions were also highly correlated (0.69).

### 3.3. Accuracy of the projected AGB and combined AGB estimate for 2016

The AGB predictions for the year 2014 were projected to 2016 with growth models (Figure 5). These  $\text{AGB}_{\text{Projected}_2016}$  estimates resulted in underestimate of  $9.9 \text{ Mg ha}^{-1}$  (7.0%) and RMSE of  $30.8 \text{ Mg ha}^{-1}$  (21.8%) with standard deviation of  $44.4 \text{ Mg ha}^{-1}$  (Table 6). When the AGB prediction model developed with 2014 data was applied to 2016 data, AGB was overestimated.  $\text{AGB}_{2016\_pred2014}$  had a bias of  $-19.6\%$  ( $-27.7 \text{ Mg ha}^{-1}$ ) and RMSE of  $33.2\%$  ( $46.9 \text{ Mg ha}^{-1}$ ). Combining the two estimates ( $\text{AGB}_{2016}$  and  $\text{AGB}_{\text{Projected}_2016}$ ) to generate an  $\text{AGB}_{\text{Combined}_2016}$  decreased the bias from  $-10.6 \text{ Mg ha}^{-1}$  ( $-7.5\%$ ) to  $-0.4 \text{ Mg ha}^{-1}$  ( $-0.3\%$ ) when compared to the most precise single

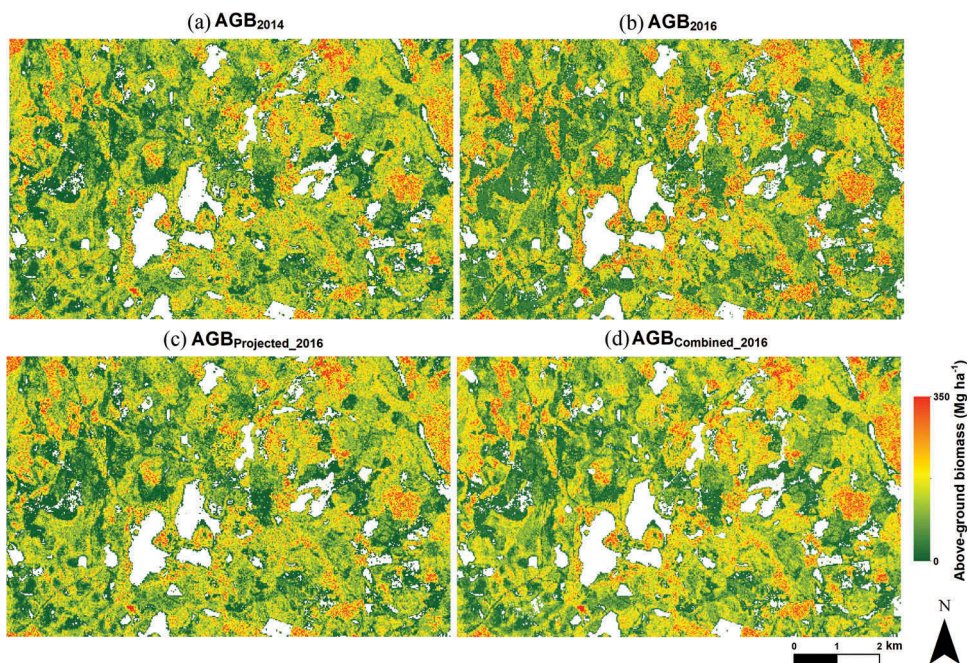


**Figure 5.** Aboveground biomass map for (a) 2014 ( $AGB_{2014}$ ) and (b) 2016 ( $AGB_{2016}$ ) as well as (c) growth-projected aboveground biomass ( $AGB_{Projected\_2016}$ ) and (d) combined aboveground biomass ( $AGB_{Combined\_2016}$ ) maps covering the study area (61.19°N, 25.11°E).  $AGB_{Projected\_2016}$  and  $AGB_{Combined\_2016}$  maps should only be used for undisturbed areas.

**Table 6.** Accuracy of the predicted aboveground biomass estimates ( $AGB_{2016}$ ), projected AGB estimates ( $AGB_{Projected\_2016}$ ), combined AGB estimates ( $AGB_{Combined\_2016}$ ), and estimates predicted using model from year 2014 ( $AGB_{2016\_pred2014}$ ) in validation sample plots ( $n = 84$ ) in 2016.  $AGB_{Combined\_2016}$  is obtained by averaging  $AGB_{2016}$  and  $AGB_{Projected\_2016}$  at the sample plot level.

	Bias (mg ha <sup>-1</sup> )	Bias (%)	RMSE (mg ha <sup>-1</sup> )	RMSE (%)	Standard deviation (Mg ha <sup>-1</sup> )
$AGB_{2016}$	-10.6	-7.5	36.7	26.0	50.6
$AGB_{Projected\_2016}$	9.9	7.0	30.8	21.8	44.4
$AGB_{Combined\_2016}$	-0.4	-0.3	29.5	20.9	45.7
$AGB_{2016\_pred2014}$	-27.7	-19.6	46.9	33.2	49.4

estimate of AGB for 2016. Similarly, the RMSE was 29.5 Mg ha<sup>-1</sup> (20.9%), improving the most accurate single date estimate from RMSE of 36.7 Mg ha<sup>-1</sup> (26.0%). The standard deviation of  $AGB_{Combined\_2016}$  was 45.7 Mg ha<sup>-1</sup>, which is in line with the single date predictions (Table 6). Based on our sensitivity test with varying weights, it was possible to improve RMSE only slightly. RMSE decreased from 20.9% to 20.4% when a weight of 0.6 was given to  $AGB_{Projected\_2016}$  and 0.4 to  $AGB_{2016}$  predictions (Figure 6). However, the lowest bias was obtained using equal weights.

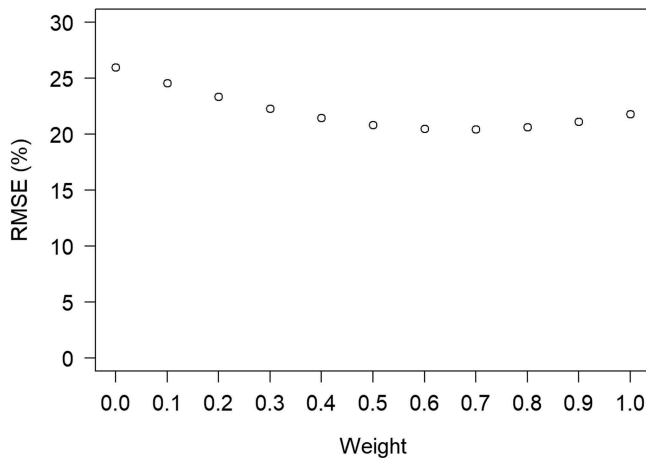


**Figure 6.** Variation in relative RMSE when projected inventory ( $AGB_{Projected\_2016}$ ) is combined with recent inventory ( $AGB_{2016}$ ) with varying weights. Weight '0.1' means that combined estimate is calculated by giving weight of '0.1' for  $AGB_{Projected\_2016}$  and '0.9' to  $AGB_{2016}$ .

#### 4. Discussion

In this study, forest AGB was predicted for 2014 and 2016 using IPCs derived from WorldView-2 stereo-imagery, AGB ground observations, and a DTM derived from ALS data. Tree-level AGB equations were used to calculate AGB for individual trees within the measured ground plots in 2014 and a total plot AGB (in  $Mg\ ha^{-1}$ ) was then calculated by summing the AGB of all the individual trees within a sample plot. To obtain the AGB reference values for the year 2016, the ground plot AGB estimates from 2014 were projected to the year 2016 following standard practices using empirical individual tree-level growth models (Hynynen et al. 2002) that are widely used in short-term forest growth updates. Thus, the quality of our AGB reference in 2014 and 2016 varied slightly as the AGB reference values used in 2016 included growth-projecting errors; however, the growth projection was performed only for 2 years and the tree-level input information based on field measurements did not include any prediction errors that are dominating short-term growth projection (Holopainen et al. 2010; Luoma et al. 2017). To provide some scale of the error sources in our study, the RMSE for  $AGB_{2014}$  was  $28.9\ Mg\ ha^{-1}$  as the expected AGB growth was  $2.1\ Mg\ ha^{-1}\ year^{-1}$ . Thus, we can assume that our reference data were suitable for our study design and our findings are not hampered by the quality of the reference data.

The accuracy of the  $AGB_{2014}$  and  $AGB_{2016}$  was 21.1% and 26.0%, respectively, at the plot level. One reason for difference is the different number of sample plots that were used in the model development for 2014 and 2016 (Table 1). Due to forest management actions in the study area, 204 sample plots were used to develop the prediction model for year 2016 as 248 sample plots were used with 2014 data. St-Onge, Hu, and Vega (2008) predicted forest AGB using sample plots, IKONOS stereo pair-derived point height metrics, an ALS-based DTM, and linear regression at a Canadian test site located close to Quebec. By using only one height-related feature (99<sup>th</sup> percentile) as a predictor for AGB, the authors obtained a Pearson correlation coefficient of 0.79 and RMSE of  $70.6\ Mg\ ha^{-1}$

(46.3%). In turn, plot-level RMSEs between 34% and 50% have been obtained for stem volume in complex structured Central European forests using IPCs derived from satellite stereo-imageries by Immitzer et al. (2016) and Straub et al. (2013). As canopy height and AGB are highly correlated and canopy height can be characterized using satellite stereo IPCs (see e.g. Persson and Perko 2016; Persson 2016), AGB was predicted in structurally rather simple boreal forest conditions even at plot level far more accurately than in more complex forest environments (Immitzer et al. 2016; St-Onge, Hu, and Vega, 2008; Straub et al. 2013). AGB prediction accuracies obtained by Yu et al. (2015) using IPC obtained from WorldView-2 stereo data in the same study site as used here (relative RMSE of 22%) and Persson (2016) using IPC obtained from Pléiades stereo data in two Swedish test sites (relative RMSE of 26%) are in line with our results.

In addition to canopy height, AGB is correlated with forest density. Changes between 2014 and 2016 in forest height were captured consistently by the imagery on undisturbed sample plots, although the expected growth in boreal forest conditions within two growth seasons is low (<1 m in height). However, the features describing forest density and variation in forest height were not as consistent. For example, canopy cover changes varied from -79.8% to 17.3% and the change in standard deviation of canopy height ranged between -5.3 m and 3.1 m. It is challenging to capture forest density or structure for any image-based techniques (Vastaranta et al. 2013; White et al. 2013; Yu et al. 2015), but it also seems that small changes in image geometry can impact these features, further contributing to inconsistencies (Wulder et al. 2008). In particular, differences in acquisition dates, solar azimuth, and viewing geometry can change the abundance and location of shadows, which in turn can impact the effectiveness of image matching algorithms (Baltsavias et al. 2008). These factors undoubtedly contributed to the variation observed in canopy cover and standard deviation of canopy height and can have implications for implementing methods over large areas covered by multiple image footprints. These factors also limited the transferability of the AGB prediction models between 2014 and 2016. Our results indicated that the most biased and inaccurate method for obtaining AGB for 2016 was to apply the prediction model that was developed using data for 2014 to data from 2016.

Nyström et al. (2015) obtained only limited improvements by using Kalman filtering in the forest attribute estimation when combining estimates from several inventory years. In our study, the most precise estimates were obtained after combining  $AGB_{Projected\_2016}$  and  $AGB_{2016}$ . The bias decreased from 7.0% ( $AGB_{Projected\_2016}$ ) and -7.5% ( $AGB_{2016}$ ) to -0.3% ( $-0.4 \text{ Mg ha}^{-1}$ ). However, combined estimates had only marginally lower RMSE. The combination of two AGB estimates did improve our results and if multi-temporal data are available, our results in this forest environment indicate that it is worthwhile to use them for estimating AGB. However, it should be noted that we validated the methods using undisturbed sample plots. Since the time interval between inventories was only two years and similar remote-sensing data were used in both 2014 and 2016 for estimation, it was expected that weights close to 0.5 would provide good results when combining AGB estimates (see e.g. Nyström et al. 2015). This was supported by our sensitivity test as the lowest bias was obtained with equal weights. Only slightly improved RMSE was possible to obtain with unequal weights in the sensitivity tests and even then the optimal weights were 0.6 and 0.4 for  $AGB_{Projected\_2016}$  and  $AGB_{2016}$ , respectively. It should be noted that although the prediction errors between the two

inventories ( $AGB_{2014}$  and  $AGB_{2016}$ ) were highly correlated (0.69), there were still sample plots with AGB below  $50 \text{ Mg ha}^{-1}$  as well as sample plots with AGB close to  $250 \text{ Mg ha}^{-1}$  that were overestimated in one year and underestimated in the other year. Therefore, an approach whereby the two AGB estimates were combined improved both accuracy and precision of the AGB estimates.

The forest height-related metrics are highly correlated with forest AGB (e.g. Kaasalainen et al. 2015; Koch 2010). Therefore, image-matched height metrics should be prioritized over spectral metrics when estimating forest structural attributes such as AGB (Persson 2016). However, while not available for our study, WorldView-2 also provides multispectral images at a GSD of 1.84 m and presumably, the use of multispectral information in addition to point clouds may have improved estimation accuracy for species-specific forest inventory attributes that were required to project the  $AGB_{2014}$  estimates for two growing seasons. Nevertheless, it has also been shown that it is more important to accurately estimate forest structural attributes such as height and diameter rather than tree species when compiling stem volume and AGB information for forest planning calculations, such as growth projection (Tompalski et al. 2014). In our study, species information was only required for the short two-season AGB projection.  $AGB_{2014}$  and  $AGB_{2016}$  estimates were obtained directly based on NN imputation and the results of these imputations were considered accurate. The accuracy of the  $AGB_{\text{Projected}_2016}$  was also in line with the accuracy of  $AGB_{2014}$  and  $AGB_{2016}$  estimates, and thus, the effect of errors in growth models in 2016 estimates should be marginal, although presumably in some sample plots, incorrect growth models may have been selected. When projecting AGB estimates for a longer time interval, it should be noted that growth simulators (e.g. Hynynen et al. 2002; Rasinmäki, Mäkinen, and Kalliovirta 2009) often require many other attributes in addition to AGB, such as tree species and site productivity, which must also be available if AGB estimates are projected. In our study,  $AGB_{2014}$  growth projection was only two growing seasons, and in addition to AGB, we imputed all the required forest inventory attributes for year 2014 to enable growth projection.

## 5. Conclusion

An increase in canopy height was detected from WorldView-2-derived IPCs acquired two years apart, providing the basis for consistent AGB predictions between two dates. However, detected changes in canopy cover and variation in tree height were not as consistent, presumably due to small changes in imaging geometry. Although there was temporal autocorrelation between the inventory errors of  $AGB_{2014}$  and  $AGB_{2016}$ , improved accuracy and precision of the AGB estimates were obtained after  $AGB_{\text{Projected}_2016}$  and  $AGB_{2016}$  estimates were combined at sample plot level ( $AGB_{\text{Combined}_2016}$ ). Compared to using only the most recent AGB predictions ( $AGB_{2016}$ ), the combination of  $AGB_{\text{Projected}_2016}$  with the  $AGB_{2016}$  using a weighted average decreased the RMSE from 26.0% to 20.9% and the bias from  $-7.5\%$  to  $-0.3\%$ . Therefore, it seems that the accuracy of short-term forest AGB estimation and mapping can be improved, relative to that of single time-point estimates, by the use of two date 3D data.



## Acknowledgments

The authors are grateful to Lic.Sc. Risto Viitala and Häme University of Applied Sciences for enabling us to conduct the research at Evo. The authors also thank the editor and reviewers for insightful comments and useful suggestions ultimately improving this research.

## Disclosure statement

The authors have no potential conflict of interest.

## Funding

This work was supported by the European Community's Seventh Framework Programme ([FP7/2007-2013]) under Grant 606971 and by the Academy of Finland under Grants 293389, 272195, and 273806.

## ORCID

Mikko Vastaranta  <http://orcid.org/0000-0001-6552-9122>  
 Ninni Saarinen  <http://orcid.org/0000-0003-2730-8892>  
 Michael A. Wulder  <http://orcid.org/0000-0002-6942-1896>  
 Joanne C. White  <http://orcid.org/0000-0003-4674-0373>  
 Henrik J. Persson  <http://orcid.org/0000-0002-3403-057X>

## References

- Axelsson, P. 2000. "DEM Generation from Laser Scanner Data Using Adaptive TIN Models." *International Archives of Photogrammetry and Remote Sensing* 33 (1): 111–118.
- Baltsavias, E., A. Gruen, H. Eisenbeiss, L. Zhang, and L. T. Waser. 2008. "High-Quality Image Matching and Automated Generation of 3D Tree Models." *International Journal of Remote Sensing* 29 (5): 1243–1259. doi:10.1080/01431160701736513.
- Breiman, L. 2001. "Random Forests." *Machine Learning* 45 (1): 5–32. doi:10.1023/A:1010933404324.
- DeVenecia, K., S. Walker, and B. Zhang. 2007. "New Approaches to Generating and Processing High Resolution Elevation Data with Imagery." In *Photogrammetric Week '07*, edited by Dieter Fritsch, 297–308. Stuttgart: Wichmann Herbert.
- Drusch, M., U. Del Bello, S. Carlier, O. Colin, V. Fernandez, F. Gascon, B. Hoersch et al. 2012. "Sentinel-2: ESA's Optical High-Resolution Mission for GMES Operational Services." *Remote Sensing of Environment* 120 (5): 25–36. doi:10.1016/j.rse.2011.11.026.
- Eitel, J. U., B. Höfle, L. A. Vierling, A. Abellán, G. P. Asner, J. S. Deems, C. L. Glennie et al. 2016. "Beyond 3-D: The New Spectrum of Lidar Applications for Earth and Ecological Sciences." *Remote Sensing of Environment* 186 (12): 372–392. doi:10.1016/j.rse.2016.08.018.
- Falkowski, M. J., M. A. Wulder, J. C. White, and M. D. Gillis. 2009. "Supporting Large-Area, Sample-Based Forest Inventories with Very High Spatial Resolution Satellite Imagery." *Progress in Physical Geography* 33 (3): 403–423. doi:10.1177/0309133309342643.
- Goetz, S. J., A. Baccini, N. T. Laporte, T. Johns, W. Walker, J. Kellndorfer, R. A. Houghton, and M. Sun. 2009. "Mapping and Monitoring Carbon Stocks with Satellite Observations: A Comparison of Methods." *Carbon Balance and Management* 4 (1): 2. doi:10.1186/1750-0680-4-2.
- Greenberg, J. A., S. Z. Dobrowski, and S. L. Ustin. 2005. "Shadow Allometry: Estimating Tree Structural Parameters Using Hyperspatial Image Analysis." *Remote Sensing of Environment* 97 (1): 15–25. doi:10.1016/j.rse.2005.02.015.

- Holopainen, M., M. Vastaranta, and J. Hyyppä. 2014. "Outlook for the Next Generation's Precision Forestry in Finland." *Forests* 5 (7): 1682–1694. doi:10.3390/f5071682.
- Holopainen, M., M. Vastaranta, J. Rasinmäki, J. Kalliovirta, A. Mäkinen, R. Haapanen, T. Melkas, X. Yu, and J. Hyyppä. 2010. "Uncertainty in Timber Assortment Estimates Predicted from Forest Inventory Data." *European Journal of Forest Research* 129 (6): 1131–1142. doi:10.1007/s10342-010-0401-4.
- Honkavaara, E., P. Litkey, and K. Nurminen. 2013. "Automatic Storm Damage Detection in Forests Using High-Altitude Photogrammetric Imagery." *Remote Sensing* 5 (3): 1405–1424. doi:10.3390/rs5031405.
- Hudak, A.T., L. C. Nicholas, J. S. Evans, D. E. Hall, and M. J. Falkowski. 2008. "Nearest Neighbor Imputation of Species-level, Plot-scale Forest Structure Attributes from LiDAR Data." *Remote Sensing of Environment* 112 (2008): 2232–2245.
- Hyde, P., R. Dubayah, W. Walker, J. Bryan Blair, M. Hofton, and C. Hunsaker. 2006. "Mapping Forest Structure for Wildlife Habitat Analysis Using Multi-Sensor (Lidar, SAR/ InSAR,ETM+, Quickbird) Synergy." *Remote Sensing of Environment* 102 (1): 63–73. doi:10.1016/j.rse.2006.01.021.
- Hynynen, J., R. Ojansuu, H. Hökkä, J. Siipilehto, H. Salminen, and P. Haapala. 2002. "Models for Predicting Stand Development in MELA System." *Finnish Forest Research Institute Research Papers* 835: 1–116
- Hyyppä, J., H. Hyyppä, D. Leckie, F. Gougeon, X. Yu, and M. Maltamo. 2008. "Review of Methods of Small-Footprint Airborne Laser Scanning for Extracting Forest Inventory Data in Boreal Forests." *International Journal of Remote Sensing* 29 (5): 1339–1366. doi:10.1080/01431160701736489.
- Immitzer, M., C. Stepper, S. Böck, C. Straub, and C. Atzberger. 2016. "Use of WorldView-2 Stereo Imagery and National Forest Inventory Data for Wall-To-Wall Mapping of Growing Stock." *Forest Ecology and Management* 359 (2016): 232–246. doi:10.1016/j.foreco.2015.10.018.
- Kaasalainen, S., M. Holopainen, M. Karjalainen, M. Vastaranta, V. Kankare, K. Karila, and B. Osmanoglu. 2015. "Combining Lidar and Synthetic Aperture Radar Data to Estimate Forest Biomass: Status and Prospects." *Forests* 6 (1): 252–270. doi:10.3390/f6010252.
- Kankare, V., M. Holopainen, M. Vastaranta, E. Puttonen, X. Yu, J. Hyyppä, M. Vaaja, H. Hyyppä, and P. Alho. 2013. "Individual Tree Biomass Estimation Using Terrestrial Laser Scanning." *ISPRS Journal of Photogrammetry and Remote Sensing* 75 (1): 64–75. doi:10.1016/j.isprsjprs.2012.10.003.
- Koch, B. 2010. "Status and Future of Laser Scanning, Synthetic Aperture Radar and Hyperspectral Remote Sensing Data for Forest Biomass Assessment." *ISPRS Journal of Photogrammetry and Remote Sensing* 65 (6): 581–590. doi:10.1016/j.isprsjprs.2010.09.001.
- Leboeuf, A., A. Beaudoin, R. A. Fournier, L. Guindon, J. E. Luther, and M.-C. Lambert. 2007. "A Shadow Fraction Method for Mapping Biomass of Northern Boreal Black Spruce Forests Using QuickBird Imagery." *Remote Sensing of Environment* 110 (4): 488–500. doi:10.1016/j.rse.2006.05.025.
- Luoma, V., N. Saarinen, M. A. Wulder, J. C. White, M. Vastaranta, M. Holopainen, and J. Hyyppä. 2017. "Assessing Precision in Conventional Field Measurements of Individual Tree Attributes." *Forests* 8 (2): 38. doi:10.3390/f8020038.
- Nyström, M., N. Lindgren, J. Wallerman, A. Grafström, A. Muszta, K. Nyström, J. Bohlin et al. 2015. "Data Assimilation in Forest Inventory: First Empirical Results." *Forests* 6 (12): 4540–4557. doi:10.3390/f6124384.
- Persson, H. J. 2016. "Estimation of Boreal Forest Attributes from Very High Resolution Pléiades Data." *Remote Sensing* 8 (9): 736. doi:10.3390/rs8090736.
- Persson, H. J., and R. Perko. 2016. "Assessment of Boreal Forest Height from WorldView-2 Satellite Stereo Images." *Remote Sensing Letters* 7 (12): 1150–1159. doi:10.1080/2150704X.2016.1219424.
- Proisy, C., P. Coutron, and F. Fromard. 2007. "Predicting and Mapping Mangrove Biomass from Canopy Grain Analysis Using Fourier-Based Textural Ordination of IKONOS Images." *Remote Sensing of Environment* 109 (3): 379–392. doi:10.1016/j.rse.2007.01.009.
- Rasinmäki, J., A. Mäkinen, and J. Kalliovirta. 2009. "SIMO: An Adaptable Simulation Framework for Multiscale Forest Resource Data." *Computers and Electronics in Agriculture* 66 (1): 76–84. doi:10.1016/j.compag.2008.12.007.
- Repola, J. 2008. "Biomass Equations for Birch in Finland." *Silva Fennica* 42 (1): 605–624. doi:10.14214/sf.236.

- Repola, J. 2009. "Biomass Equations for Scots Pine and Norway Spruce in Finland." *Silva Fennica* 43 (1): 625–647. doi:10.14214/sf.184.
- Song, C. 2013. "Optical Remote Sensing of Forest Leaf Area Index and Biomass." *Progress in Physical Geography* 37 (1): 98–113. doi:10.1177/0309133312471367.
- St-Onge, B., Y. Hu, and C. Vega. 2008. "Mapping the Height and Above-Ground Biomass of a Mixed Forest Using Lidar and Stereo Ikonos Images." *International Journal of Remote Sensing* 29 (5): 1277–1294. doi:10.1080/01431160701736505.
- Straub, C., J. Tian, R. Seitz, and P. Reinartz. 2013. "Assessment of Cartosat-1 and WorldView-2 Stereo Imagery in Combination with a LiDAR-DTM for Timber Volume Estimation in a Highly Structured Forest in Germany." *Forestry* 86 (4): 463–473. doi:10.1093/forestry/cpt017.
- Tompalski, P., N. C. Coops, J. C. White, and M. A. Wulder. 2014. "Simulating the Impacts of Error in Species and Height upon Tree Volume Derived from Airborne Laser Scanning Data." *Forest Ecology and Management* 327 (9): 167–177. doi:10.1016/j.foreco.2014.05.011.
- Vastaranta, M., I. Korpela, A. Uotila, A. Hovi, and M. Holopainen. 2012. "Mapping of Snow-Damaged Trees Based on Bitemporal Airborne LiDAR Data." *European Journal of Forest Research* 131 (4): 1217–1228. doi:10.1007/s10342-011-0593-2.
- Vastaranta, M., M. Niemi, M. A. Wulder, J. C. White, K. Nurminen, P. Litkey, E. Honkavaara, M. Holopainen, and J. Hyypä. 2016. "Forest Stand Age Classification Using Time Series of Photogrammetrically Derived Digital Surface Models." *Scandinavian Journal of Forest Research* 31 (2): 194–205. doi:10.1080/02827581.2015.1060256.
- Vastaranta, M., M. A. Wulder, J. C. White, A. Pekkarinen, S. Tuominen, C. Ginzler, V. Kankare, M. Holopainen, J. Hyypä, and H. Hyypä. 2013. "Airborne Laser Scanning and Digital Stereo Imagery Measures of Forest Structure: Comparative Results and Implications to Forest Mapping and Inventory Update." *Canadian Journal of Remote Sensing* 39 (5): 382–395. doi:10.5589/m13-046.
- White, J. C., M. A. Wulder, M. Vastaranta, N. C. Coops, D. Pitt, and M. Woods. 2013. "The Utility of Image-Based Point Clouds for Forest Inventory: A Comparison with Airborne Laser Scanning." *Forests* 4 (3): 518–536. doi:10.3390/f4030518.
- Wulder, M. A., J. C. White, R. F. Nelson, E. Næsset, H. O. Ørka, N. C. Coops, T. Hilker, C. W. Bater, and T. Gobakken. 2012b. "Lidar Sampling for Large-Area Forest Characterization: A Review." *Remote Sensing of Environment* 121 (6): 196–209. doi:10.1016/j.rse.2012.02.001.
- Wulder, M. A., J. G. Masek, W. B. Cohen, T. R. Loveland, and C. E. Woodcock. 2012a. "Opening the Archive: How Free Data Has Enabled the Science and Monitoring Promise of Landsat." *Remote Sensing of Environment* 122 (7): 2–10. doi:10.1016/j.rse.2012.01.010.
- Wulder, M. A., R. J. Hall, N. C. Coops, and S. E. Franklin. 2004. "High Spatial Resolution Remotely Sensed Data for Ecosystem Characterization." *BioScience* 54 (6): 511–521. doi:10.1641/0006-3568(2004)054[0511:HSRRSD]2.0.CO;2.
- Wulder, M. A., S. M. Ortley, J. C. White, and N. C. Coops. 2008. "Impact of Sun-Surface-Sensor Geometry upon Multitemporal High Spatial Resolution Satellite Imagery." *Canadian Journal of Remote Sensing* 34 (5): 455–461. doi:10.5589/m08-062.
- Yu, X., J. Hyypä, H. Kaartinen, and M. Maltamo. 2004. "Automatic Detection of Harvested Trees and Determination of Forest Growth Using Airborne Laser Scanning." *Remote Sensing of Environment* 90 (4): 451–462. doi:10.1016/j.rse.2004.02.001.
- Yu, X., J. Hyypä, M. Karjalainen, K. Nurminen, K. Karila, M. Vastaranta, V. Kankare et al. 2015. "Comparison of Laser and Stereo Optical, SAR and InSAR Point Clouds from Air-And Space-Borne Sources in the Retrieval of Forest Inventory Attributes." *Remote Sensing* 7 (12): 15933–15954. doi:10.3390/rs71215809.
- Yu, X., X. Liang, J. Hyypä, V. Kankare, M. Vastaranta, and M. Holopainen. 2013. "Stem Biomass Estimation Based on Stem Reconstruction from Terrestrial Laser Scanning Point Clouds." *Remote Sensing Letters* 4 (4): 344–353. doi:10.1080/2150704X.2012.734931.
- Zhang, B., S. Miller, K. DeVenecia, and S. Walker. 2006. "Automatic Terrain Extraction Using Multiple Image Pair and Back Matching." *ASPRS 2006 Annual Conference*.
- Zolkos, S. G., S. J. Goetz, and R. Dubayah. 2013. "A Meta-Analysis of Terrestrial Aboveground Biomass Estimation Using Lidar Remote Sensing." *Remote Sensing of Environment* 128 (1): 289–298. doi:10.1016/j.rse.2012.10.017.